CO-DESIGN OF VERY FLEXIBLE ACTUATED STRUCTURES

Salvatore Maraniello[1], Rafael Palacios[1]
[1] Imperial College, London, SW7 2AZ, United Kingdom
r.palacios@imperial.ac.uk

Keywords: Optimisation, Co-design, MDO, GEBM, Single-shooting, Control Vector Parametrisation, Open-loop control, MDSDO

Abstract: A numerical investigation on open-loop control and combined structural and control design (co-design) of very flexible beams is presented. The objective is to allow for an efficient design of these systems by identifying design strategies that provide significant performance advantages with respect to conventional sequential design methods. The control vector parametrisation method, implemented for both a B-splines (local) and discrete sines (global) set of basis functions, is used in conjunction with a gradient based optimiser to solve first the open-loop control and then the co-design problems. Numerical results show the impact of the time-frequency resolution of the parametrisation on the outcome of the optimisation. Overall, B-splines can achieve higher performance as they better exploit the flexible, high frequency driven, behaviour of the structure, particularly as large deformations lead to changes in the natural frequencies of the system. The discrete sines based parametrisation, on the other hand, is found to be a more robust choice. The mutual influence between control and structural dynamics during the design process is showed and used to explain the ability of the optimiser to approach a global optimum. In particular, it was found that control and structural disciplines can freeze the design around specific characteristic frequencies (*locking*), limiting the advantages of a co-design approach based on gradient methods.

Nomenclature

Acronyms

CVP Control vector parametrisation

DSS Discrete sine series

FoR Frame of reference

fps Frames per second

GEBM Geometrically-exact beam model

Greek Symbols

ρ Material density

τ_n n-th control point used for the B-splines parametrisation

Roman Symbols

A Body-attached frame of reference

B Local frame of reference defined along the beam mean axis s

c Column vector for the optimisation problems constrains

EI Beam bending stiffness

f_0 Fundamental frequency in the DSS parametrisation and step in frequency between consecutive sine waves

f_n Frequency of n-th sine wave in the DSS parametrisation

f_{max} Maximum frequency captured by the parametrisation of the control

G Global frame of reference

I Cost function for the optimisation problems

l_2, l_3 Sides of the beam rectangular cross-section

m Order of B-spline basis

M_Y Applied external moment used for the pendulum optimal control and co-design

N_τ Number of control points for the B-spline parametrisation

N_c Size of the basis used to parametrise the control

P Penalty term used for the compound pendulum optimal control and co-design

R Residual form of the physical system

s Beam mean axis

T Final time of the dynamic simulations

t Time

u Control function

v_X Beam tip X velocity measured in the global frame of reference G

x Column vector containing the design variables for the optimisation problems

y Physical system state

Subscripts

c Control related quantities in co-design problems

s Structural related quantities in co-design problems

1 INTRODUCTION

Feedback control strategies to enhance vehicle aeroelastic performance are increasingly important in aircraft design. While active systems generally provide better performance than non-controlled, or passive, ones, the integration of the controller usually comes late in the design process. Most airframes are designed using a sequential approach: in an early stage development the structure is typically sized for passive response and an active control is introduced only in a later stage, after the main features of the system have been established [1]. Looking at the design process from the perspective of a multidisciplinary optimisation problem, there is substantial evidence that this approach is likely to generate only sub-optima design points [2, 3].

Historically, aeronautical design has been characterised by relatively stiff structures exhibiting small deformations. The deriving low influence of the structural geometrical changes on control systems performance has, therefore, justified the use of a sequential approach, particularly when considering the practical advantages of decoupling analysis and optimisation process. Novel aeronautical components, such as high altitude long endurance (HALE) aircraft wings or large horizontal axis wind turbine (HAWT) blades are, however, characterised by the presence of highly flexible structures, whose large deformations lead to nonlinear dynamical responses. As most of the critical operating conditions of these systems - both in terms of loading and stability - are associated with unsteady phenomena, an accurate representation of the coupled (aeroservoelastic) dynamics is a necessary, but not sufficient, condition to achieve optimal designs. For a true optimum, structural properties and feedback control should be designed simultaneously, thus leading to the concept of combined design (co-design).

The advantages of a combined control and structural optimisation were already proved by early work in space structures design [4, 5] and in robotics [6]. These studies used a linear representation of the closed loop system dynamics, which facilitated the approach to the design. Asada et al. [6], for instead, directly manipulated the position of the closed-loop system eigenvalues, while Rao [5] expressed the optimiser gains in terms of the system energy properties. In this sense, the work from Onoda and Haftka [4] is the first one to best fit the modern idea of combined design, as, aside from trying a nested approach similar to that presented by Rao [5], they also optimised the system simultaneously with respect to optimiser gains and structural design parameters. However, when dealing with more expensive models, particularly on the structural side, the integration of optimisation methodologies for the two disciplines has proven to be a difficult task. A crucial point is to ensure a balanced modelling, in terms of fidelity, between control and structural analysis disciplines while containing the overall computational cost.

This necessity is a common leitmotiv of multidisciplinary optimisation (MDO). In aerospace applications, however, MDO has so far mainly been applied to the development of efficient methods (coupled adjoints) for static aerostructural optimisation and, thus, structural tailoring for passive response. While on one side this tendency is linked to the fact that industrial design still relies strongly on passive analysis methodologies, the increasing computational cost associated with dynamic analysis and optimisation has been another important factor to limit the MDO applications in dynamic problems. The sensitivity analysis presents a further issue, given the relatively high modelling cost of developing adjoint methods for nonlinear structural dynamics models [7]. The problem of co-design has been more recently attacked in the aeroservoelasticity domain to optimise physical systems parameters and feedback control gains of novel aircraft for loads allevia-

tion under gust or manoeuvres. In these cases, however, reduced order structural models and linearised formulations were used [8, 9]. Integrated design approaches dealing with complex structural models have been limited to the use of metamodels [10] in robotics or to small size systems [11].

As recognised in a recent review by Allison and Herber [3], the lack of emphasis on systems dynamics is a general issue of common MDO architecture. In particular, the authors underlined that for controlled systems, the optimisation/design process should explicitly account for the fact that one discipline, the control one, is inherently dependent on the evolution of a system in time. This consideration is leading to the development of a new branch of MDO, the multidisciplinary dynamic system design optimisation (MDSDO).

From a structural perspective, the analysis of HALE vehicles wings or large HAWT blades introduces nonlinearities when dealing with large geometrical deformations. For HALE wing design, moreover, the coupling between rigid-body and flexible modes dynamics needs to be accounted for [12]. From a control system perspective, open-loop analysis is a necessary step for a large class of problems, such as trajectory control and manoeuvre design. In real life applications, these problems need to be addressed in the presence of disturbances and thus the need of feedback control and closed-loop analysis. A deterministic open-loop analysis, in which the control has full authority on the system behaviour, remains, however, a necessary first step in the development process. Also for the design of feedback control systems, optimal control analysis frees the design process from the assumption of any specific control architecture, thus allowing to explore a larger state-design space or to better assess the performance of a given control architecture [13].

Optimal control problems can be solved through an optimise-discretise approach, in which an optimality condition is enforced on the equations describing the system dynamics. However, in real life applications, the system is often too complex to apply optimality principles. A common way around this problem is to parametrise the control signal (direct methods). Single and multiple shooting methods, in particular, are directly linked to single and multidisciplinary optimisation: once a parametrisation is chosen, the coefficients of the parametrisation are directly handled by the optimisation algorithm and there is no formal difference, at the optimiser level, between closed loop system gain optimisation and open-loop optimal control solution.

While single and multiple shooting methods have been successfully used in many optimal control problems, an understanding on how these methods may apply to the control of active, strongly nonlinear, structures, is a required step to assess the feasibility of their use in a co-design framework. The most common tendency within the control community is to use piecewise constant or linear representations [14]. This choice can be acceptable from a control system design perspective — as a simplified model for the physical systems is often used — but often not when a balanced modelling fidelity is sought. In this case, more refined parametrisations, capable to produce realistic signals, should be used — for example to ensure first derivative continuity in the control input. The first aim of this work is, therefore, to shed light on this point, assessing how different parametrisations perform for problems in which the system feature change in time due to nonlinear effects.

The single shooting (or control vector parametrisation, CVP) method can be integrated in a pre-existing MDO architecture with relatively little effort. There is, however, little understanding on how this would perform for a combined optimisation process. As most of high fidelity optimisation models rely on gradient based methods, in particular, it is important to asses whether the smoothness of the design space is compromised when

passing from optimal control to combined design.

To this aim, a coupled flexible-rigid body dynamics model, based on a geometrically exact beam model (GEBM) has been embedded in an optimisation framework. The actuation on the structure is written as an optimal control problem using both a local (B-spline) and a global (discrete sine series, DSS) parametrisation. The methodology is used to control the dynamics of a very flexible beam in hinged configuration and exhibiting large deformations. As the beam flexibility increases, the level of coupling between rigid and flexible modes increases as well. Conceptually, therefore, this problem has many analogies to that of the trajectory control of flexible aircraft in calm air. The active system co-design is then faced: given the high level of coupling, a multidisciplinary feasible (MDF) architecture [2] is used. While the architecture implemented do not explicitly exploits the time nature of the system, control and structure are both modelled on similar fidelity level, thus allowing the optimiser to fully exploit the features of the system.

2 MODEL AND METHODOLOGY

The optimisation framework is tested for the control and co-design of the flexible pendulum proposed in Ref. [7] and whose structural properties are described in Sec. 3.2. This problem is fully deterministic, as no external disturbances are accounted for, and has large affinity with that of the trajectory control of a very flexible aircraft. The pendulum, in fact, can exhibit large deformations — comparable in magnitude with its length —, particularly during the co-design phase, when the performance of very flexible structures can be explored by the optimiser. Importantly, not only the large deformations but also the coupling between flexible and rigid body modes need to be captured.

This sections starts introducing the structural GEBM with coupled rigid-flexible body dynamics (Sec. 2.1). The problem of optimal control of the pendulum is then faced, with Sec. 2.2 providing a brief introduction to direct methods for nonlinear optimal control and their relation with *standard* optimisation architectures. The control vector parametrisations or single shooting method is discussed in more details in Sec. 2.3, where the discretisations implemented in this work are also presented. The section closes with an overview of the optimisation framework built for control and co-design (Sec. 2.4).

2.1 Rigid-flexible body dynamic model

For modelling the pendulum a GEBM with coupled rigid-flexible body dynamics [15, 16] is used. The model is here briefly described using the notation introduced in Ref. [17]; frame of references (FoRs) and relevant vectors are shown in Fig. 1. The rigid body dynamics is expressed in terms of translational (v_A) and rotational (ω_A) velocity vectors of a FoR attached to the body, A, in respect to the ground FoR G[1]. Local deformations are assumed to be small, thus a linear material model is used. Force and moment strains are written in terms of position $R_A(s)$ and the Cartesian rotation vector $\Psi(s)$ associated to a local FoR B, defined along the beam mean axis s [15]. The coupled nonlinear rigid body dynamics is finally expressed using:

$$M(\eta) \left\{ \begin{array}{c} \ddot{\eta} \\ \dot{\beta} \end{array} \right\} + \left\{ \begin{array}{c} Q^s_{gyr}(\eta, \dot{\eta}, \beta) \\ Q^r_{gyr}(\eta, \dot{\eta}, \beta) \end{array} \right\} + \left\{ \begin{array}{c} Q^s_{stif}(\eta) \\ 0 \end{array} \right\} = \left\{ \begin{array}{c} Q^s_{ext}(\eta, \zeta, t) \\ Q^r_{ext}(\eta, \zeta, t) \end{array} \right\} , \qquad (1)$$

[1]Note that, according to Ref. [17], the subscript stands for the FoR in which quantities are projected.

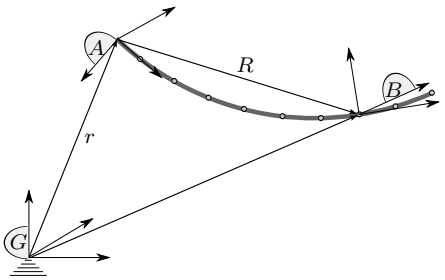

Figure 1: Definition of frames of reference

where $\beta^T = \left\{v_A^T, \omega_A^T\right\}$, η is a vector containing nodal rotation and displacements, and Q_{gyr}, Q_{stiff}, Q_{ext} are, respectively, gyroscopic, stiffness and external forcing terms. Note that the external force Q_{ext} includes both the control input and the gravitational force. In particular, the orientation of the FoR A, ζ, is required. This is expressed in terms of quaternions such that $\zeta^T = \{\zeta_0, \zeta_v^T\}$. The scalar ($\zeta_0$) and vector ($\zeta_v$) parts of ζ are obtained via integration of the FoR A angular velocity ω_A according to [18, 19]:

$$\dot{\zeta_0} = -\frac{1}{2}\omega_A^T\zeta_v \quad , \quad \dot{\zeta_v} = -\frac{1}{2}\left(\zeta_0\omega_A - \tilde{\omega}_A\zeta_v\right) \tag{2}$$

where ($\tilde{}$) is the skew symmetric matrix operator.

Spherical joint boundary conditions (BCs) have been implemented by setting the velocity of the body FoR v_A to be zero. Hinge BCs can be derived similarly, allowing rotations only along one axis; a validation is presented in Sec. 3.1.

2.2 From optimal control to co-design

From a general point of view, an optimal control problem can be seen as an optimisation problem in which the design variable is a time-dependent function, the control input $u(t)$:

$$\begin{aligned} \text{minimise} \quad & I = I(u, y, \dot{y}) \\ \text{with respect to} \quad & u(t), y(t) \\ \text{subject to} \quad & c_c(u, y) \geq 0 \\ & R(t, u, y, \dot{y}) = 0 \end{aligned} \tag{3}$$

In problem (3) y is the state of the system[2], I is the cost functional to minimise while c and R define design and discipline constraints. In the current work, in particular, the set of equations R is linked to the solution of a GEBM given in eq. (1) over the time domain (*time horizon*) $[0, T]$. The design constraints c, instead, refer to specific requirements for the control. In this work, *bound constraints* of the form

$$u_L(t) \geq u(t) \geq u_H(t) \quad t \,\epsilon\, [0, T] \tag{4}$$

[2]Note that the notation used here follows the common standard used in optimisation, thus diverging from the typical notation used in control theory.

as well as initial and terminal values are enforced.

Analytical tools for the solution of problem (3) are available: an optimality condition, as the Pontryagin's maximum principle (PMP), is usually enforce and the control $u(t)$ is derived either analytically or, most commonly, numerically. Such approaches, usually referred to as indirect methods, are, however, too complex to be used for the control of large nonlinear systems [3, 14]. In direct methods, the control function is discretised in time and expressed in terms of a coefficient vector x_c, i.e. $u(t) = u(x_c)$. In direct transcription (DT) or direct simultaneous methods, also the state is discretised in time and treated as a design variable. The optimiser, therefore, handles problem (3) directly, thus solving the physical and optimal control problem simultaneously. In a MDO context, this approach would be referred to as All At Once (AAO) architecture. While DT deriving methods are capable of exploring infeasible and unstable states, thus possibly leading to a faster convergence of the optimisation, the number of design variables is drastically increased. Convergence issues, when integrating the approach in a MDO architecture, are also likely to arise.

If eq. (1) is solved at each iteration for the state y, problem (3) can be recast in the form of a multidisciplinary feasible architecture (MDF):

$$\begin{aligned} \text{minimise} \quad & I = I(x_c, y(x_c), \dot{y}(y(x_c), x_c)) \\ \text{with respect to} \quad & x_c \\ \text{subject to} \quad & c(x_c, y(x_c)) \geq 0 \end{aligned} \tag{5}$$

where the dependency of the state on the control $y = y(x_c)$ has been underlined. This approach is referred to as control vector parametrisation (CVP) or single-shooting method: while a solution to eq. (1) has to be found at each optimisation, the size of the optimisation problem is reduced to its minimum. The extension of problem (5) to a MDO problem that simultaneously optimises control action and structural design parameters is straightforward and only requires the inclusion of structural design parameters x_s and structural constraints c_s:

$$\begin{aligned} \text{minimise} \quad & I = I(x_c, x_s, y(x_c, x_s), \dot{y}(y, x_c, x_s)) \\ \text{with respect to} \quad & x_c, x_s \\ \text{subject to} \quad & c_c(x_c, x_s, y(x_c, x_s)) \geq 0 \\ & c_s(x_c, x_s, y(x_c, x_s)) \geq 0 \end{aligned} \tag{6}$$

2.3 Control parametrisation

In most control problems, the control u is parametrised with a piecewise constant approximation. In addition to being easy to implement, this scheme offers good convergence properties and allows for discontinuity, which are necessary to model some types of control (e.g. bang-bang control, [14]). In order to model accurately the movement of typical control actuators for aeronautical applications (e.g. the deflection of aerodynamic control surfaces) while limiting the size of the coefficients used x_c, a $\mathcal{C}^1$ continuous or higher parametrisation is required.

Clearly, the quality of the optimal control largely depends on the choice of the parametrisation [20]. Other then being realistic, this should be somehow capable of capturing the

features of the system to be controlled. In particular, the dynamics of structures is strongly linked to the frequency of excitations of external disturbances, as well as control forces. It is thus natural to use a parametrisation that can be easily linked to the frequency range that the control can exhibit.

An obvious candidate is the Discrete Fourier series (DFS) or, for control signals having $u(0) = u(T) = 0$, a Discrete Sine series (DSS), that is,

$$u(t) = \sum_{n=1}^{N_c} x_{cn} \sin 2\pi f_n t \quad \text{with:} \quad f_n = n\ f_0\ \ , \quad f_0 = \frac{1}{2T} \tag{7}$$

The DFS and DSS have both the advantage of allowing a direct control of the maximum actuation frequency of the control. While they are globally defined in time, however, the frequency resolution depends on the time horizon T. For DFS series, the frequency step is $f_0 = \frac{1}{T}$, while for DSS is $f_0 = \frac{1}{2T}$. A poor frequency resolution can be an issue when trying to capture the features of structural dynamical problems, particularly when dealing with large deformations and nonlinear structures. In trying to exploit or control resonance phenomena, for instance, the control may be required to include specific narrow frequency ranges. For very flexible systems, moreover, not only the natural frequency of the modes may change during the simulation if deformations become large, but the distance between the characteristic frequency of different modes (both rigid and flexible) can also drastically reduce.

The duality frequency vs. time resolution is a well known problem in signal and image processing [21]. In this sense, local basis functions can provide more flexibility in terms of capturing relevant frequency content of the structural dynamics response, including when nonlinearities imply changes of the system features in time. B-splines, in particular, have been chosen for their smoothness properties. A set of B-splines basis functions of order p can be built recursively over a set of N_τ control points τ_n as [20]:

$$\phi_n^{(0)}(t) = \begin{cases} 1 & \text{if } \tau_n < t < \tau_{n+1} \\ 0 & \text{else} \end{cases} \tag{8}$$

and

$$\phi_n^{(p)}(t) = \frac{t - \tau_n}{\tau_{n+p} - \tau_n}\phi_n^{(p-1)}(t) + \frac{\tau_{n+p+1} - t}{\tau_{n+p+1} - \tau_{n+1}}\phi_{n+1}^{(p-1)}(t) \quad p > 0 \tag{9}$$

Note that, if N_τ control points are used, the number of spline basis required is $N_c = N_\tau + p - 1$. The control signal $u(t)$ is thus expressed as:

$$u(t) = \sum_{n=1}^{N_c} x_{cn}\ \phi_n^{(p)}(t) \tag{10}$$

Based on Nyquist criterion, in order to capture a maximum frequency f_{max}, at least 2 control points per wave are necessary. Convergence studies showed that third order B-splines provide good and smooth reconstructions for the application in this work. These have been, therefore, chosen as a good compromise between locality of the function[3] and smoothness[4].

For both basis, bound constraints are enforced either analytically (B-splines) or by oversampling the control signal (DFS and DSS).

[3] As the splines order increases, in fact, the number of control points required for each wave increases as well.

[4] Note, however, that for a good representation of all the frequencies up to f_{max}, at least 4 control points per wave should be used;

2.4 Optimisation and framework

A gradient based method will be used to solve both the nonlinear optimal control and the co-design optimisation. The choice of a gradient method is a compromise between the need to keep the computational costs down, the objective of the optimisation and the design space to explore. When using medium-high fidelity models and dealing with dynamics a global reconstruction of the design space is in general not a feasible solution. On the other hand, once the main features of the system are defined, the design space does not require to be explored blindly but, on the contrary, a certain design needs to be refined. The assumption of local convexity is therefore expected to be a valid one. While gradient based methods are often used in optimal control [20, 22], however, this approach has to be further explored when dealing with co-design problems, particularly in understanding how the convexity of the design space, and thus the solution found, is affected when switching from optimal control to co-design.

In this work, a SLSQP optimisation algorithm is used [23]. The GEBM with coupled flexible-rigid body dynamics from an in-house aeroelastic simulation environment (SHARPy — simulation of high aspect ratio planes, [17, 24, 25]) has been embedded in an optimisation framework built using OpenMDAO [26]. The implementation is monolithic and uses finite differences for the gradient evaluation.

3 NUMERICAL INVESTIGATIONS

This section starts presenting the flexible pendulum model and a verification of the GEBM implementation. The optimisation framework and the CVPs introduced are then exercised for the optimal control case proposed in Ref. [7] and results are compared under similar optimisation objectives (Sec. 3.2). In order to show the effect of using different discretisations, the behaviour of two pendula of different flexibility is analysed. A Design of experiment (DOE) is then performed: for a fixed DSS and spline parametrisation of the control input, the optimal control problem is solved for structures of different flexibility (Sec. 3.3). Finally, the co-design is attempted using a gradient based method, and the quality of the results is assessed.

3.1 Model description and verification

The flexible pendulum configuration proposed in Ref. [7] is sketched in Fig. 2. The pendulum, modelled as a hinged elastic beam, has a constant rectangular cross-section along its length; the material properties, as well as the specific dimensions of the cross-section, however, are varied from case to case to obtain stiffer or more flexible designs.

Results obtained with the hinged configuration have been compared against the free falling flexible beam case proposed in Ref. [7] (Fig. 3). The beam here presented has a total mass of 1 kg and an overall length of 1 m. Mass and stiffness properties are constant along its span, with bending stiffness $EI = 0.15$ kg m^2, negligible rotatory inertia and infinite extensional stiffness. A gravity value of 9.80 m s^2 has been used. The beam tip displacements show a good comparison against the results presented in Ref. [7].

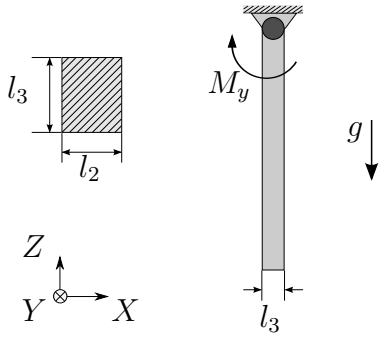

Figure 2: Flexible pendulum geometry

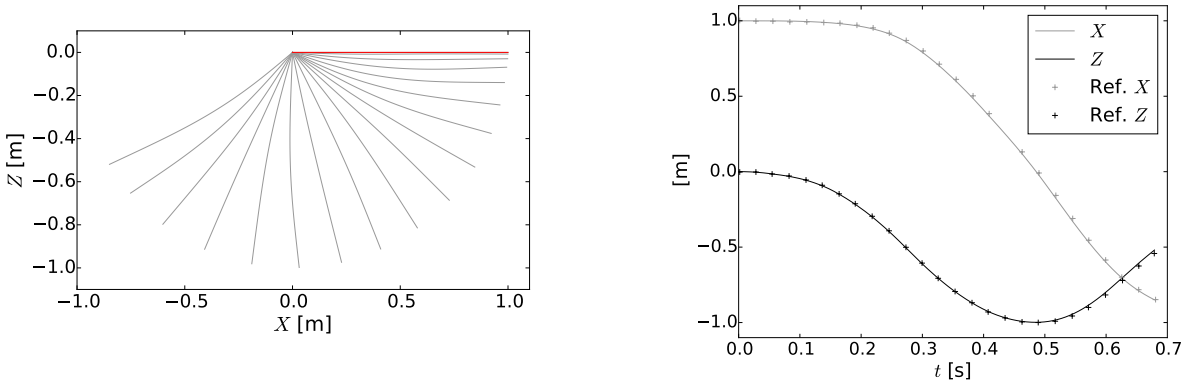

(a) Snapshots of deformed beam

(b) Tip position time history against Ref. [7]

Figure 3: Free falling hinged flexible beam (the beam is horizontal at time $t = 0$ s).

3.2 Optimal control results

In the optimal control problem proposed in Ref. [7] the pendulum is initially in a stable equilibrium position along the vertical direction (Z axis); gravity effects are accounted for. A control torque moment, $M_Y(t)$, chosen to be zero at the initial and final time of the simulation, is applied at its root (Fig. 2), causing the pendulum to oscillate about the hinge point. The torque time history $M_Y(t)$ is optimised such to maximise the leftward X velocity of the pendulum tip, v_X, measured in the global FoR G at time $T = 2$ s. Note that, in spite of the X axis orientation in the global FoR G, v_X is assumed to be positive when pointing leftward, such to ease the analysis of the numerical investigations. The problem so presented is fully deterministic and can be written, in its continuous form, as:

$$\begin{aligned} \text{minimise} \quad & \kappa_1 \, v_X + \kappa_2 \, P(M_Y) \\ \text{with respect to} \quad & M_Y(t) \\ \text{subject to} \quad & M_Y(0) = M_Y(T) = 0 \\ & -M_{max} < M_Y(t) < M_{max} \end{aligned} \tag{11}$$

where

$$P(M_Y) = \frac{1}{2}\int_0^T \left[\pi_1 \; M_Y^2 + \pi_2 \; \left(\frac{dM_Y}{dt}\right)^2\right] dt$$

is a penalty term for the control input. In the numerical implementation, M_Y is discretised by mean of eq.s (7) and (10) when using, respectively, a DSS and a spline basis parametrisation; the optimisation is thus performed with respect to basis functions coefficients x_c. The constants κ_i and π_i are scaling parameters to ensure that all the terms in the cost function and penalty factor have same units and comparable magnitude; note that κ_1 is required to have negative value. An isotropic material of Young's module $E = 1.2$ Pa and density $\rho = 100$ kg m^{-3} was used; the beam has length $L = 1$ m and a constant rectangular cross-section of area $A = 10^{-2}$ m^2 with negligible rotatory inertia [7]. In the results presented in this work, rigid body rotations and deformations are all planar; thus the only relevant elastic quantity is the bending stiffness about the local axis perpendicular to the plane where displacements occur. Two beams of different bending stiffness, one 10 times stiffer then the other, are obtained varying the sides of the cross-section l_2 and l_3 as summarised in Tab. 1. In the following, the two pendula are referred to as *stiff* and *flexible*.

Case	l_2 [m]	l_3 [m]	EI [Nm^2]	f_r [Hz]	f_b [Hz]
stiff pendulum	0.1000	0.1000	10.0	0.50	7.76
flexible pendulum	0.3162	0.0316	1.0	0.50	2.45

Table 1: Pendula structural properties for the optimal cases proposed in Ref. [7].

As the mass properties do not vary, the rigid-body frequency linked to the period of large free oscillation of the pendulum, f_r, is unchanged from one case to another. As the structure becomes more flexible, however, the natural frequency related to the first bending mode f_b is drastically reduced[5] (Tab. 1). While from a physical point of view this implies a larger coupling with the rigid body mode, from a control point of view it is important to ensure that the frequency resolution of the control parametrisation is enough to capture the different modes. For the DSS parametrisation, for example, the step in frequency between waves is $f_0 = 0.25$ Hz, thus showing that as the structure becomes more flexible not only coupling effects increase, but becomes also harder for the control to target specific modes.

For both the case proposed in Tab. 1 the optimal control problem is solved with B-spline and DSS parametrisations of different basis sizes, based on the maximum frequency, f_{max}, captured by the control; for the B-spline parametrisation, in particular, the Nyquist criterion was used to estimate it. It is worth noticing that, fixed a certain value of f_{max}, the size of DSS and B-spline basis are comparable. In particular, for each parametrisation the basis size was chosen such to include and exclude the flexible mode natural frequency of vibration. In both cases, the control input was bounded not to exceed an absolute value of $M_{max} = 3.5$ N m; the cost and penalty term parameters were set as per Ref. [7] to be:

$$\kappa_1 = -1 \text{ s m}^{-1} \quad , \quad \kappa_2 = 1$$

[5]The characteristic frequencies in Tab. 1 have been computed assuming an underformed configuration for f_r and an Euler-Bernoulli beam model under the small vibrations hypothesis. While large deformations imply changes in the characteristic frequencies of the structure as it deforms, these values still give a relevant idea of where the resonance points are located in the frequency domain.

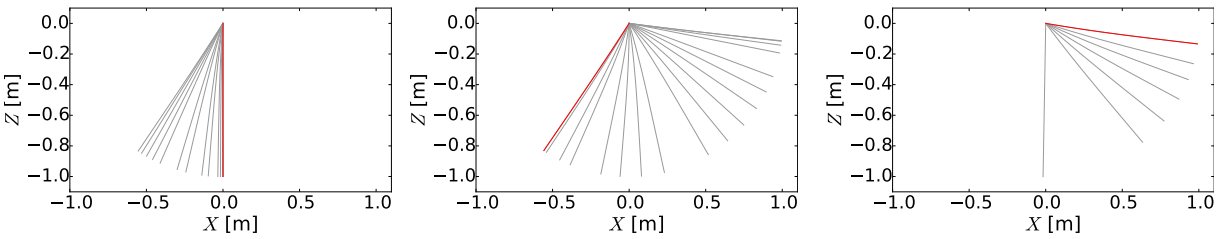

(a) $t \in [0.00", 0.72"]$ (b) $t \in [0.72", 1.60"]$ (c) $t \in [1.60", 2.00"]$

Figure 4: Snapshots (25 frames per second) of the *stiff* pendulum response for the optimal actuation with a control maximum frequency $f_{max} = 2$ Hz using a DSS parametrisation.

$$\pi_1 = 1 \text{ N}^{-2}\text{m}^{-2}\text{s}^{-1} \quad , \quad \pi_2 = 10^{-2} \text{ N}^{-2}\text{m}^{-2}\text{s}$$

3.2.1 *Stiff* pendulum

For the *stiff* pendulum case the parametrisations have been chosen as shown in Tab. 2. In the table, N_c and f_{max} refer to the basis size of each parametrisation and the related maximum frequency of actuation. The number of iterations, NI, required to complete the optimisations and the resulting cost (I), penalty factor (P) and final pendulum tip velocity (v_X) values are also presented.

Parametrisation	N_c	f_{max} [Hz]	NI	v_X[ms^{-1}]	P	I
spline	11	≈ 2	20	6.0838	2.7349	-3.3489
DS	8	2	14	6.0783	2.7257	-3.3525
spline	43	≈ 10	33	12.3490	6.1835	-6.1655
DS	40	10	44	10.5722	4.7685	-5.8036

Table 2: Optimal control of the *stiff* pendulum using different parametrisations.

As it can be seen, for the cases in which $f_{max} = 2$ Hz, the control moment does not excite the first bending mode of the pendulum, which, therefore, only swings rigidly. This is reflected in Fig. 4, where the snapshots of the pendulum response to the optimal actuation (modelled using a DSS) show no relevant elastic deformation. The optimal control and tip displacements related to the $f_{max} = 2$ Hz cases have been compared against Ref. [7] in Fig. 5. Both the spline and DSS parametrisation can capture well the rigid-body motion frequency, thus returning very similar performances. As physically expected, the control moment excites the rigid-body motion and uses the gravity potential energy to increase the final tip velocity v_X while limiting the penalty term P.

Setting $f_{max} > f_b$ leads to a drastic improvement of performance as the first bending mode is now excited. From an energy analysis point of view, the active system is now capable of storing not only kinetic (rigid-body motion) but also elastic energy; this is returned at the end of the simulation to enhance the performance. While both the discretisations show to be capable to exploit the system physics, the spline parametrised control achieves an extra 6% reduction in cost function. The splines local nature, in fact, allows the control to better adjust on the natural bending frequency of the beam, particularly when, as the deformations become larger (Fig. 6), this changes during the simulation. As a result, while the final cost I is similar for the two cases, the spline based control based results show a larger, but justified, magnitude of the penalty value P.

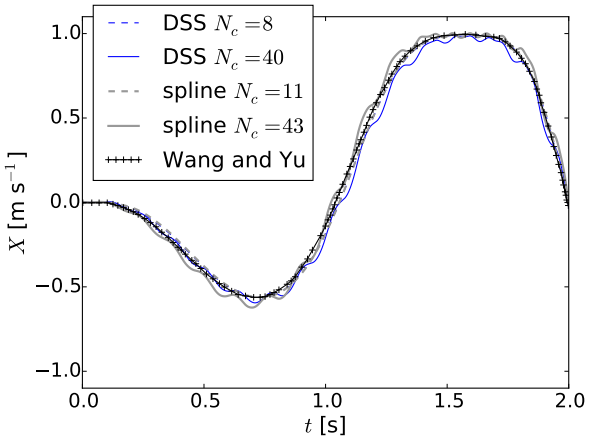

(a) Tip horizontal position

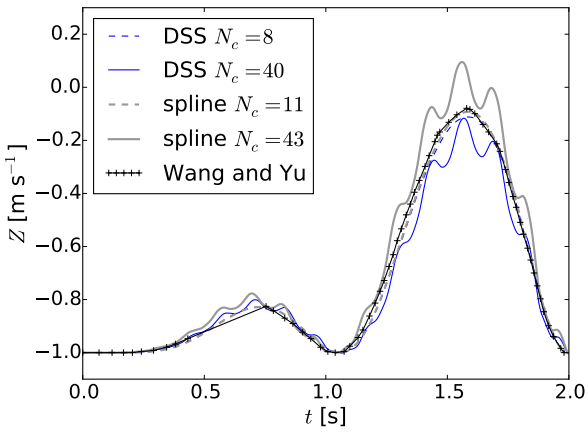

(b) Tip vertical position

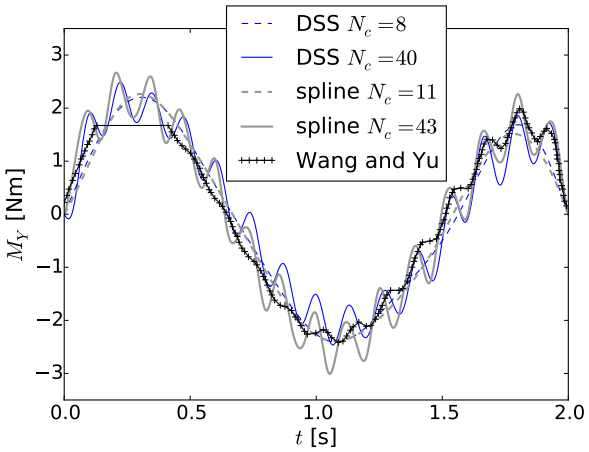

(c) Torque moment M_Y

Figure 5: Results for the optimal control of the *stiff* pendulum using different parametrisations. The comparison is against the optimisation results obtained by Wang and Yu [7].

3.2.2 *Flexible* pendulum

As the pendulum flexibility is increased, the distance between rigid and flexible body characteristic frequencies f_r and f_b is drastically reduced and it becomes harder to excite one of the modes without exciting the others. Also, geometrically nonlinear deformations imply changes in the characteristic frequencies of the system. Setting and results for the optimal control are summarised in Tab. 3; as for the *stiff* pendulum case, the discretisations are chosen such to exclude ($f_{max} = 1.5$ Hz) and include ($f_{max} = 4$ Hz) the pendulum bending mode natural frequency ($f_b = 2.5$ Hz).

The effect of the higher coupling rigid-flexible dynamics can be seen in the results obtained when limiting the control maximum frequency to $f_{max} = 1.5$ Hz. The B-spline parametrised control returns a very smooth M_Y time history, with a very low magnitude and penalty term P. The DS discretisation, instead, manages to excite the first bending mode, thus achieving better performances. In both cases, the optimal control provides physically valid results as both discretisations capture, as expected, the rigid-body dynamics. The higher nonlinearity of the system, however, encourages the proliferation of local minima or, more generally, of solutions that depend on the evolution of the control torque M_Y during optimisation. The concept is underlined in Fig. 8, where the M_Y signal obtained after one iteration of the optimisation is shown. While the B-spline parametrisa-

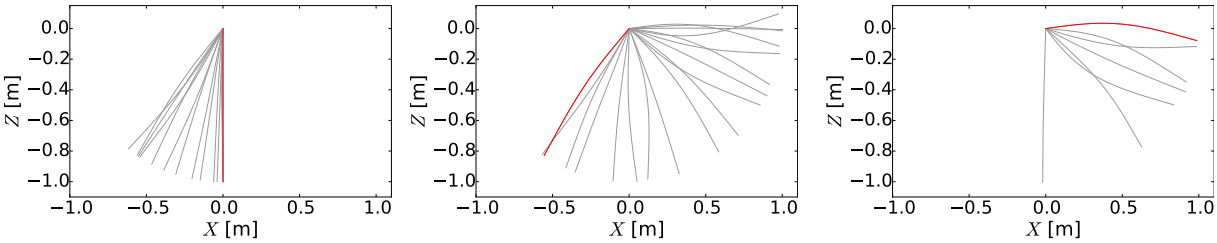

(a) $t \in [0.00", 0.72"]$ (b) $t \in [0.72", 1.60"]$ (c) $t \in [1.60", 2.00"]$

Figure 6: Snapshots (25 fps) of the *stiff* pendulum response for the optimal actuation obtained using a B-spline parametrisation with $N_c = 43$ control points ($f_{max} = 10$ Hz).

tion leads to a slow increases of the torque magnitude, the DSS parametrisation produces strong control forces that enhance higher deformations in the beam (Fig. 8). The bending mode is excited (coupling flexible-rigid body dynamics), thus allowing the optimiser to *see* the flexible body dynamics and drive the solution towards a point where the elastic behaviour of the pendulum is also exploited.

When the size of the control basis is increased such that $f_{max} > f_b$, both the discretisations can capture the flexible dynamics regardless of the path towards solution. Even in this case, spline basis provide better performance: as deformations are relevant, these manage to better exploit the resonance, as the frequency of excitation can be adjusted during the simulation. The DSS discretisation, moreover, suffers of frequency resolutions issues, as the step between consecutive waves $f_0 = 0.25$ Hz — dictated by the parametrisation scheme, eq. (7) — is almost comparable to the distance between rigid and flexible modes frequencies.

Parametrisation	N_c	f_{max} [Hz]	NI	v_X [ms^{-1}]	P	I
spline	9	≈ 1.5	22	5.3981	2.1882	-3.2099
DS	6	1.5	40	8.4210	4.5029	-3.9181
spline	19	≈ 4	57	15.9226	5.7340	-10.1887
DS	16	4	53	13.1122	3.4838	-9.6284

Table 3: Optimal control of the *flexible* pendulum using different parametrisations.

3.2.3 Some conclusions

In all the cases shown, results agree well with those obtained by Ref. [7] (see Fig. 5 and 7). The results in Ref. [7] are obtained using Chebyshev polynomials and a beam model accounting for damping. This latter difference becomes more important for the *flexible pendulum* case, where the current results clearly show higher actuation (Fig. 7c) in order to exploit the system resonance. It was also seen that different parametrisations can produce different result: the maximum frequency captured by the control and — when the nonlinearity of the system increases — the path followed by the optimiser are the main influencing factors.

When the system nonlinearity increases, as a dependency of the final control on the path towards the optimum is seen, gradient methods should be used with special care. While a physically valid solution was always obtained, global basis seem more capable to capture the system behaviour even when the parametrisation has an insufficient number of bases functions ($f_{max} < f_b$). From one point of view, this is linked to the fact that the

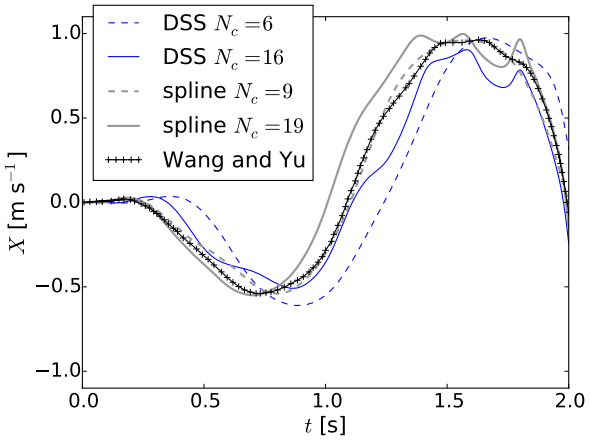

(a) Tip horizontal position

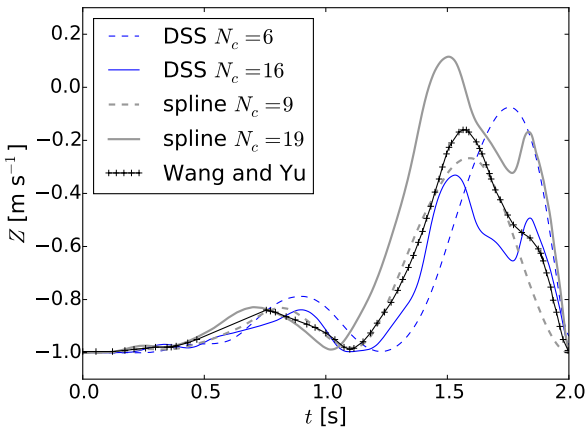

(b) Tip vertical position

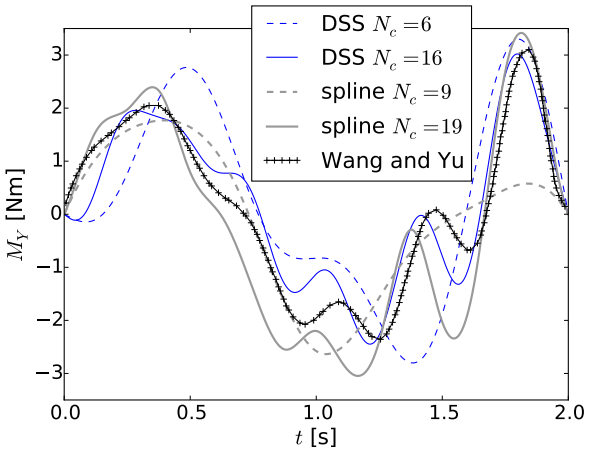

(c) Torque moment M_Y

Figure 7: Results for the optimal control of the *flexible* pendulum using different parametrisations. The comparison is against the optimisation results obtained by Wang and Yu [7].

change of the optimal torque M_Y from one step to another is more violent, thus implying that a larger design space region is explored — this comes, however, at the price of a more unstable optimisation process. From another perspective, however, this is also linked to the fact that global basis better capture the low frequency driven dynamics.

For refined enough parametrisations ($f_{max} > f_b$), the results obtained with B-splines exploit better the system resonance. Local basis, in fact, can provide a better time-frequency resolution, particularly when the system properties (in this case the flexiblity, i.e. the characteristic frequencies) change in time (nonlinear effect). This is particularly true for high frequency driven behaviour, which is localised in time and thus demands a local reconstruction.

3.3 Design of experiments: stiffness vs. control

Before attempting the active system co-design, the optimal control problem of the pendulum is solved for a range of beams of different stiffness. As shown in Sec. 3.2, if the maximum frequency f_{max} that the control can capture is fixed, a more flexible pendulum is generally expected to have better performance. For both the DSS and B-spline

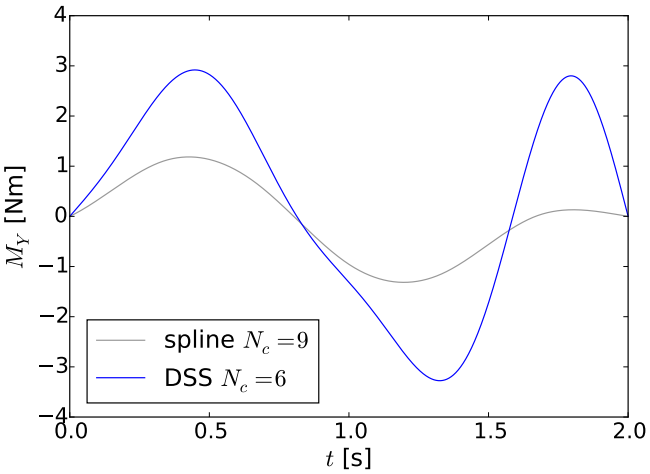

Figure 8: Optimal control after first iteration for *flexible* pendulum case using B-splines ($N_c = 9$) and a DSS ($N_c = 6$).

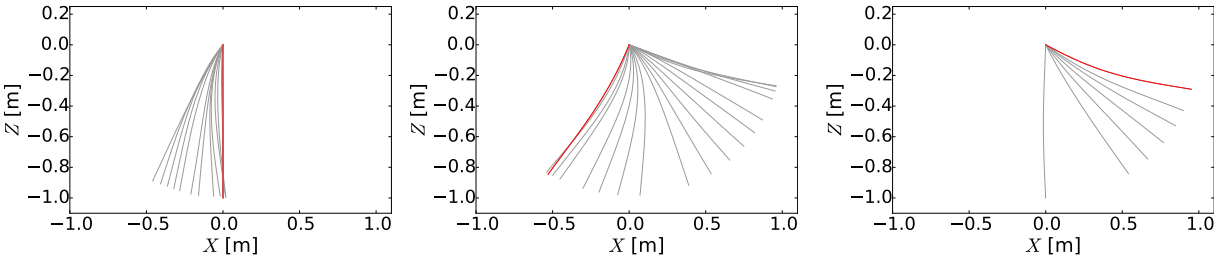

(a) $t \in [0.00", 0.72"]$ (b) $t \in [0.72", 1.60"]$ (c) $t \in [1.60", 2.00"]$

Figure 9: Snapshots (25 fps) of the *flexible* pendulum response for the optimal actuation obtained using a B-spline parametrisation with $N_c = 9$ control points ($f_{max} = 1.5$ Hz).

parametrisations, the number of basis functions is chosen such to achieve a maximum frequency $f_{max} = 6$ Hz. The resulting basis size are, respectively, 24 and 27 thus leading to a FD based sensitivity analysis of comparable computational cost. The pendulum bending stiffness is varied by changing the dimension of the beam cross-section l_2 and l_3 (Fig. 2). Note that, in order to keep the total mass — and thus the beam cross-sectional area — constant, only one of the two structural parameters is actually independent. Changes of beam bending stiffness EI and natural frequencies are summarised in Fig. 11. The structural design space, in particular, is chosen to include both designs for which the control maximum frequency f_{max} is greater and smaller of the pendulum first bending mode natural frequency. The lower bound for the beam stiffness is, furthermore, chosen such as to avoid the resonance of the second bending mode of the beam. While this could also be beneficial, it was not included in this exploratory study to simplify the analysis of the results.

Results of the DOE using a DSS parametrisation with $N_c = 24$ coefficients are presented in Fig. 12a. While the actuation penalty is fairly constant over the design space, the final tip velocity v_X and cost function values I have a steep improvement as the natural frequency of the first bending mode f_b enters in the range of the control ($l_3 = 0.0773$ m, $EI = 5.9785$ Nm^2). Fig. 12b shows, for each of the structural designs explored in the DOE, the magnitude x_{ci} of the sine waves parametrising the related optimal control.

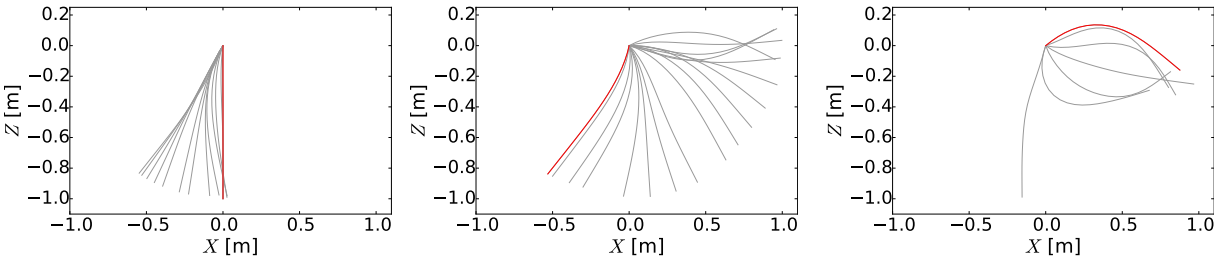

(a) $t \in [0.00", 0.72"]$ (b) $t \in [0.72", 1.60"]$ (c) $t \in [1.60", 2.00"]$

Figure 10: Snapshots (25 fps) of the *flexible* pendulum response for the optimal actuation obtained using a B-spline parametrisation with $N_c = 19$ control points ($f_{max} = 4$ Hz).

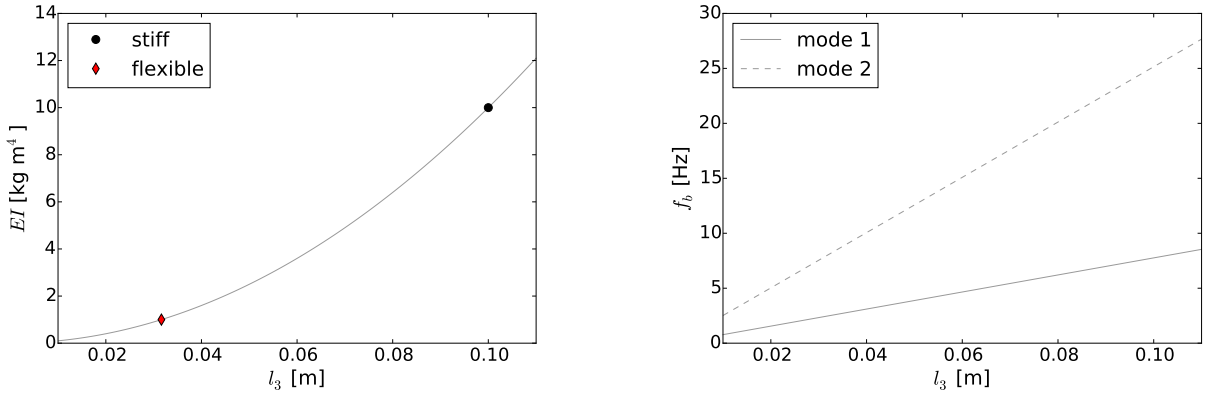

(a) Bending stiffness EI.

(b) Bending modes natural frequency for initial configuration.

Figure 11: Beam properties changes as a function of the cross-sectional shape; for each l_3 value, the size l_2 is adjusted such to keep the overall beam mass constant.

When $f_b > 6$ Hz, the optimal controls mainly have a low frequency component, such as to excite the rigid-body mode. As soon as f_b enters in the control range, however, a peak around this frequency appears. As the beam flexibility decreases, the peak position moves to follow the bending mode natural frequency. Once $l_3 < 0.070$ m, I and v_X reach a plateau: for all these different designs, in fact, both rigid and flexible dynamics are exploited, thus performance do not vary considerably.

The DOE using B-spline basis of size $N_c = 27$, shows similar trends for cost, penalty and final velocity (Fig. 13). The transition from rigid to rigid-flexible dynamics is, however, smoother. This result is in line with what was already seen in Sec. 3.2.2: when the bending frequency of the beam is outside, yet close, to the maximum frequency captured by the control, local basis struggle to capture the flexible dynamics property of the system. A further consideration is, however, required; while according to Nyquist assumption the spline basis used can express a maximum frequency of 6 Hz, the wave reconstruction achieved is not perfect, as only two control points per wave are used. As at least 4 control points per maximum frequency wave would be required to ensure a good reconstruction through the frequency range, inputs above 3 Hz are not well represented with the current parametrisation, thus providing a further explanation for the smooth trend shown in the transition region. Also the out of trend peaks in penalty term P and final velocity v_X at $l_3 = 0.080$ m can be interpreted in this optic: being the control unable

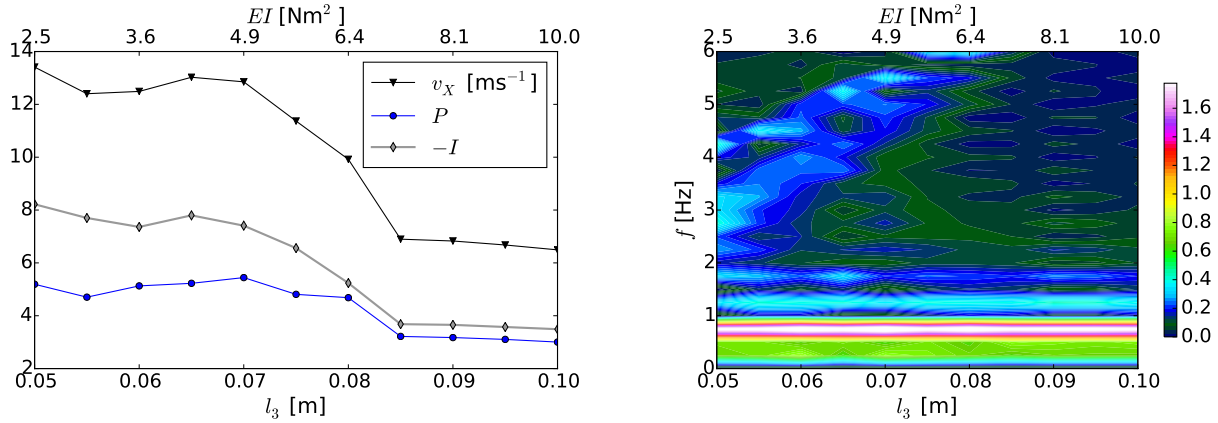

(a) DOE

(b) Optimal controls frequency content

Figure 12: DOE and optimal controls frequency content using a DSS parametrisation with $N_c = 24$ ($f_{max} = 6$ Hz).

to tune precisely with the bending mode natural frequency, a increase in the final velocity magnitude can be achieved only with a higher control force. Once the bending mode frequency is well within the frequency range of the spline parametrisation, performance become comparable to those obtained for the DSS series.

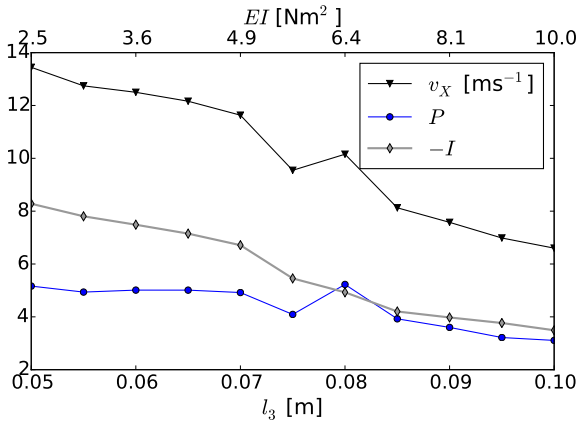

Figure 13: DOE using a B-splines basis with $N_c = 27$ ($f_{max} = 6$ Hz).

3.4 Active system co-design

For all the co-design cases considered in this section, the initial beam rectangular cross-section (Fig. 2) is set to have a relatively high bending stiffness ($EI = 6.4$ Nm^2); the initial size is $l_2 \times l_3 = 0.080 \times 0.125$ m^2, with l_3 bounded to be $l_3 \in [0.050\text{ m}, 0.200\text{ m}]$ during the co-design. Each parametrisation has been tried with different basis size, reaching a maximum frequency f_{max} of 4 Hz, 6 Hz (as per DOEs, Fig. 12a and 13) and 12 Hz. Results have been summarised in Tab. 4 and 5, comparing them to the performance obtained solving the optimal control only problem for the initial beam geometry (DOE

label in the tables). In the co-design cases, *zero* and *opt* have been used to underline the initial condition (IC) given to the control moment M_Y. For the *opt* case, in particular, the initial M_Y was set to be the optimal control found during the DOE; a zero IC for M_Y was otherwise used. Both the DOEs and physical analysis provide good confidence in the fact that the structural design is expected, in all cases, to move towards a more flexible beam, such to allow the control to exploit the first bending mode resonance.

I.C.	N_c	f_{max} [Hz]	l_3 [m]	f_b [Hz]	P	v_X [ms^{-1}]	v_X %	I	I %
zero	16	4	0.0747	5.80	3.133	6.827	5.8%	-3.694	6.4%
zero	24	6	0.0745	5.78	4.114	10.465	5.5%	-6.352	21.3%
zero	48	12	0.0790	6.13	3.085	8.471	-22.4%	-5.385	-15.9%
opt	16	4	0.0821	6.37	3.02	6.672	3.4%	-3.652	5.2%
opt	24	6	0.0800	6.21	4.683	9.92	0.0%	-5.237	0.0%
opt	48	12	0.0800	6.21	4.509	10.914	0.0%	-6.406	0.0%
DOE	16	4	0.0800	6.21	2.981	6.453	—	-3.472	—
DOE	24	6	0.0800	6.21	4.684	9.92	—	-5.237	—
DOE	48	12	0.0800	6.21	4.509	10.915	—	-6.406	—

Table 4: Results of the combined optimisation problem using DSS control parametrisations of different basis size. Percentage values are in respect to the optimal control only case (DOE).

As shown in Tab. 4, using a DSS parametrisation and starting from a zero initial torque always leads to a more flexible, thus potentially better, design. However, the stiffness reduction is not as large as expected: a minimum value of $l_3 = 0.0745$ m is achieved ($N_c = 24$ case), while the DOE shows that a global optimum is expected in the region $l_3 < 0.070$ m. For the $N_c = 24$ case, the l_3 size is reduced until $f_b \approx 6$ Hz, such as to excite the bending mode. Once this is in resonance, however, the control force and the structural design *lock* into a local minimum. Further changes in the structure lead to a degeneration of performance (as we move away from a resonance condition) and vice-versa: changes in the M_Y, and thus in its frequency content, mean a reduction in resonance as well. A local minimum is, thus, found by the gradient-based optimisation. A similar phenomenology can be seen for the $N_c = 16$ case: here the f_b is close but not yet inside the control range: however, as also seen in Sec. 3.2, the bending mode can still be excited, thus leading to locking. The $N_c = 48$ is, in this sense, the worse case: here, the control f_{max} is already larger then the first bending mode frequency: the *locking* occurs very early in the optimisation, and the structural design does not change much. The bending mode is excited but the beam flexibility does not increase as expected.

The last case also underlines issues related to the dependency of the results on the path taken by the optimiser. While, in fact, the structural design is not significantly changed, performance is worse then in the pure optimal control case, with a final cost 16% higher. The difference in the optimal M_Y for these cases is underlined in Fig. 14, where the magnitude of the sine waves used to parametrise the solution is plotted against their frequency. In particular, the co-design solution tries to minimise the final cost by pointing towards a control that excites less the rigid body motion and returns, therefore, a smaller penalty factor P. This behaviour is linked to both the form chosen for the cost function itself — as the penalty term appears explicitly — and the poor time-frequency resolution of the DSS parametrisation, which introduces noise in the design space. While

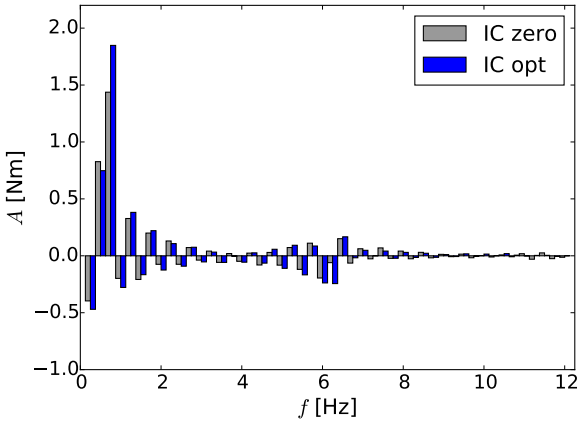

Figure 14: DSS coefficients of the optimal torque deriving from co-design and optimal control only cases.

the beam characteristic frequencies vary smoothly during the simulation (due to the large deformations) and the optimisation, the parametrisation, having a fixed frequency step $f_0 = 0.25$ Hz, can excite very differently two similar designs.

The *locking* phenomenon becomes more evident when the IC for M_Y is that obtained via optimal control solution. Here the structural design almost never changes and the optimisation stops at the very beginning. The $N_c = 16$ case, in spite the slight change in structural design, also follows the same trend. The initial torque, in fact, exploits the rigid body modes only: the structural design is, therefore, driven towards a stiffer structure, such that all the energy is used for the rigid body motion. The poor progress obtained using as IC the M_Y found via optimal control solution also proves the potential disadvantages of using a sequential design for this class of problems. If a sequential optimisation was carried on, in fact, the optimisation would stop progressing as the gradient, in this case, would be the same as per the co-design case, but without the terms related to the sensitivity with respect to the control parameters.

I.C.	N_c	f_{max} [Hz]	l_3 [m]	f_b [Hz]	P	v_X [ms^{-1}]	v_X %	I	I %
zero	19	4	0.0550	4.27	6.080	12.73	99.3%	-6.65	90.5%
zero	27	6	0.0690	5.35	4.588	10.866	7.0%	-6.278	27.4%
zero	51	12	0.0817	6.35	1.378	5.182	-60.3%	-3.805	-47.0%
opt	19	4	0.0886	6.88	2.963	6.636	3.9%	-3.673	5.2%
opt	27	6	0.0800	6.21	5.197	10.124	-0.3%	-4.927	0.0%
opt	51	12	0.0800	6.21	5.862	13.046	0.0%	-7.184	0.0%
DOE	19	4	0.0800	6.21	2.896	6.386	—	-3.49	—
DOE	27	6	0.0800	6.21	5.226	10.155	—	-4.929	—
DOE	51	12	0.0800	6.21	5.862	13.046	—	-7.184	—

Table 5: Results of the combined optimisation problem using B-spline control parametrisations of different basis size. Percentage values are in respect to the optimal control only case (DOE).

Tab. 5 shows the analogous results obtained using B-splines to parametrise the control. When the IC is set to zero and the f_{max} of the control is below the bending mode natural

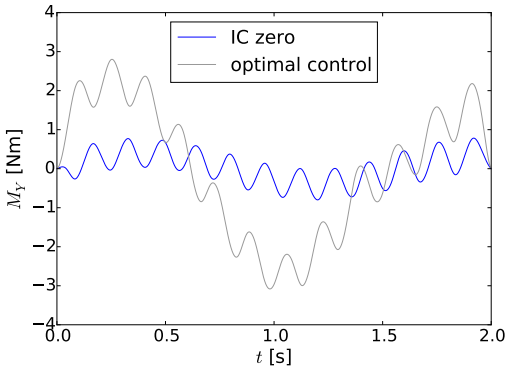

(a) Final torque

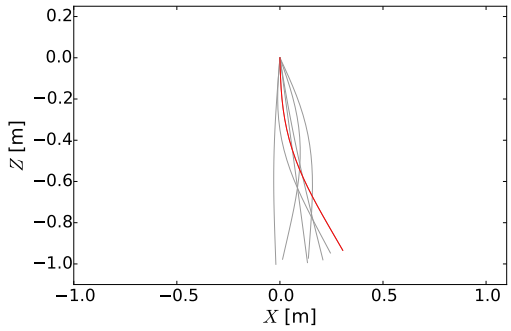

(b) Snapshots (25 fps), co-design from IC *zero*, $l_3 = 0.817$ m, $t \in [1.60", 2.00"]$

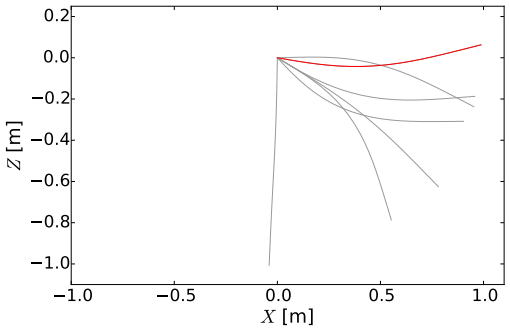

(c) Snapshots (25 fps), only optimal control, $l_3 = 0.800$ m, $t \in [1.60", 2.00"]$

Figure 15: Comparison of results from co-design (IC *zero*) and pure optimal control of the unchanged pendulum using B-splines ($N_c = 51$).

frequency f_b, the combined optimisation is capable of driving the structural design to a configuration where the control (with its limitations in terms of maximum frequency resolution), can fully exploit the physical properties of the system. In both the $N_c = 19$ and $N_c = 27$, in fact, the flexibility of the structure is increased until the natural frequency of the bending mode enters within the maximum frequency range of the control. As for the DSS parametrisation, here *locking* occurs and the optimisation stops. Nonetheless, the new design shows good improvement, particularly for the $N_c = 19$ case, where the final pendulum tip velocity almost doubles and the system flexibility is fully exploited.

When $f_b < f_{max}$, as in the $N_c = 51$ case, *locking* happens at the very beginning of the optimisation, leading to a solution in which only the bending mode resonance is exploited (Fig. 15). This poses a real issue when co-design is attempted with basis functions localised in time, as one needs to ensure that global effects, i.e. low frequencies determined behaviours, are captured as well. The analogous optimal control case (DOE in Tab. 5), on the other had, reaches a good solution: the fixed structural properties, thus, add an extra constraint in the enlarged structural-control design space that avoids the solution to get stuck in the local minimum solution showed in Fig. 15a and 15b.

Even with B-splines based control, the co-design starting from an optimal control solution shows not to progress from the IC used ($N_c = 24, 51$). As for the DSS cases, due to the presence of resonance, structural design and control start from a locked position, thus no descending path is found. Only the non-resonant case ($N_c = 17$) shows some

progresses. The dynamics, however, does not change from rigid to rigid-flexible, and the solution is only refined. As per the DSS analogous case, the structure is stiffened, such to limit the energy input in the flexible mode and increase the energy transferred to the rigid body mode.

Overall, regardless the parametrisation used, the combined optimisation starting from a *zero* torque IC led to an improved design whenever the initial bending mode of the pendulum was outside the frequency range of the control. In these cases, the process was able to drive the pendulum towards a design compatible with the control features. Improvements are more modest using a DSS parametrisation (final cost decreases up to 21%) and much larger using B-splines, where the basis local nature allowed to better exploit the resonance. The increase in performance was, however, limited by the *locking* phenomenon. This contributed to the poor performance of the co-design cases starting from *zero* torque IC when the control could excite the bending mode of the pendulum from the very start. For these cases other issues, namely the basis locality for B-splines parametrisation and the poor frequency resolution of the DSS, were found. The form of the cost function, moreover, has been seen to allow *path dependent* solutions. *Locking* also prevented the co-designs started with an optimal torque IC to progress, proving the unsuitability of a sequential approach for this problem. As for the optimal control cases, global basis seem to be more robust, as they never failed in our investigation to capture the rigid-flexible dynamics of the system. Local spline basis, on the other hand, can achieve better performance.

4 CONCLUSIONS

The control vector parametrisation technique has been used to solve the nonlinear optimal control problem — aiming to maximise the tip velocity of an elastic pendulum actuated at its hinge — of a very flexible structure and to carry out a co-design of the open-loop control and the structural properties of the system. The pendulum has been modelled using a GEBM with coupled flexible-rigid body dynamics. The problem, while fully deterministic, has been chosen to represent key features of the trajectory control of a very flexible aircraft, particularly in terms of the nonlinearities introduced by the coupled rigid-flexible body dynamics. In all cases, a gradient method has been used to drive the optimisation. The control has been modelled using B-splines and DSS, to test the effect of using local and global sets of basis functions. In both the optimal control and the co-design cases the time-frequency resolution of the parametrisations has been shown to be the most relevant factor driving the design.

The optimal control application has been tested for two beams of different stiffness to investigate the effect of an increasing rigid-flexible body dynamics coupling on the optimisation. The DSS basis proved to better extrapolate the global system behaviour, but offers a poorer time-frequency resolution. In this sense, when the basis size was large enough, B-splines showed to provide better performance, particularly when large deformations caused the system properties to change during the trajectory. As the system nonlinearity increases, a dependency of the optimal control on the path taken by the optimiser has been, furthermore, shown.

In the co-design problem, a number of factors were found to influence the final outcome of the process. Whenever the control maximum frequency resolution, f_{max}, was below the initial characteristic flexible frequency of the physical system f_b, the combined optimisation always managed to drive the structural design in a region where the control system

could correctly exploit the coupled rigid-flexible dynamics. Particularly when using B-splines, performance were found to increase considerably. Improvements in the design showed, however, to be limited by the fact that structural and control design parameters tend to *lock* the system around local minima whenever structure and control tune on the same resonance/excitation frequency. This issue is linked to the use of a gradient based method and, possibly, to the deterministic nature of the system, as no external excitations (with the characteristic frequencies connected to them) influence the system dynamics. Due to the *locking*, co-design attempts starting from a previously computed optimal control solution (which can be shown to be equivalent to a sequential design approach) showed no relevant design improvement. The quality of the solution was also compromised in the co-design cases starting from a *zero* IC if the control frequency resolution would allow to capture the flexible behaviour of the physical system from the very beginning of the optimisation. Here *locking* was most noticeable when using a B-splines parametrisation, where the control could not capture the global, low frequency driven, behaviour of the system. The DSS parametrisation showed, instead, to be more robust.

5 ACKNOWLEDGEMENT

The authors are both grateful for the sponsorship of the UK Engineering and Physical Science Research Council (EPSRC) and an EPSRC access grant to the ARCHER UK National Supercomputing Service (http://www.archer.ac.uk).

References

[1] Xu, J. and Kroo, I., "Aircraft Design with Active Load Alleviation and Natural Laminar Flow," *Journal of Aircraft*, Vol. 51, No. 5, Sept. 2014, pp. 1–14.

[2] Martins, J. R. R. A. and Lambe, A. B., "Multidisciplinary Design Optimization: A Survey of Architectures," *AIAA Journal*, Vol. 51, No. 9, 2013, pp. 2049–2075.

[3] Allison, J. and Herber, D. R., "Multidisciplinary Design Optimization of Dynamic Engineering Systems," *AIAA Journal*, Vol. 52, No. 4, April 2014, pp. 691–710.

[4] Onoda, J. and Haftka, R., "An Approach to Structure/Control Simultaneous Optimization for Large Flexible Spacecraft," *AIAA Journal*, Vol. 25, No. 8, 1987, pp. 1133–1138.

[5] Rao, S. S., "Combined Structural and Control Optimization of Flexible Structures," *Engineering Optimization*, Vol. 13, No. 1, 1988, pp. 1–16.

[6] Asada, H., Park, J., and Rai, S., "A Control-Configured Flexible Arm: Integrated Structure Control Design," *Proceedings of the 1991 IEEE International Conference on Robotics and Automation*, edited by IEEE, Sacramento, California, 1991, pp. 2356–2362.

[7] Wang, Q. and Yu, W., "Sensitivity Analysis of Geometrically Exact Beam Theory (GEBT) Using the Adjoint Method with Hydra," *52nd AIAA/ASME/ASCE/AHS/ASC Structures, Structural Dynamics and Materials Conference*, Denver, Colorado, April 2011, pp. 1–15.

[8] Haghighat, S., Martins, J. R. R. A., and Liu, H. H. T., "Aeroservoelastic Design Optimization of a Flexible Wing," *Journal of Aircraft*, Vol. 49, No. 2, March 2012, pp. 432–443.

[9] Jackson, T. and Livne, E., "Integrated Aeroservoelastic Design Optimization of Actively Controlled Strain-Actuated Flight Vehicles," *AIAA Journal*, Vol. 52, No. 6, June 2014, pp. 1105–1123.

[10] Nishigaki, H. and Kawashima, K., "Motion Control and Shape Optimization of a Suitlike Flexible Arm," *Structural optimization*, Vol. 15, 1998, pp. 163–171.

[11] Cardoso, J. B., Moita, P. P., and Valido, A. J., "Design and Control of Nonlinear Mechanical Systems for Minimum Time," *Shock and Vibration*, Vol. 15, No. 3-4, 2008, pp. 315–323.

[12] Cesnik, C. E., Palacios, R., and Reichenbach, E. Y., "Reexamined Structural Design Procedures for Very Flexible Aircraft," *Journal of Aircraft*, Vol. 51, No. 5, Sept. 2014, pp. 1580–1591.

[13] Allison, J. T., Guo, T., and Han, Z., "Co-Design of an Active Suspension Using Simultaneous Dynamic Optimization," *Journal of Mechanical Design*, Vol. 136, No. 8, June 2014, pp. 14.

[14] Lin, Q., Loxton, R., and Teo, K. L., "The Control Parameterization Method for Nonlinear Optimal Control: a Survey," *Journal of Industrial and Management Optimization*, Vol. 10, No. 1, Oct. 2013, pp. 275–309.

[15] Hodges, D. H., "A Mixed Variational Formulation Based on Exact Intrinsic Equations for Dynamics of Moving Beams," *International Journal of Solids and Structures*, Vol. 26, No. 11, 1990, pp. 1253–1273.

[16] Geradin, M. and Cardona, A., *Flexible Multibody Dynamics: A Finite Element Approach*, John Wiley & Sons Ltd, Chichester, UK, 2001.

[17] Hesse, H. and Palacios, R., "Reduced-Order Aeroelastic Models for Dynamics of Maneuvering Flexible Aircraft," *AIAA Journal*, Vol. 52, March 2014, pp. 1–16.

[18] Stevens, B. and Lewis, F., *Aircraft Control and Simulation*, John Wiley & Sons, New York, NY, USA, 1992.

[19] Palacios, R., "Nonlinear Normal Modes in an Intrinsic Theory of Anisotropic Beams," *Journal of Sound and Vibration*, Vol. 330, No. 8, 2011, pp. 1772–1792.

[20] Schlegel, M., Stockmann, K., Binder, T., and Marquardt, W., "Dynamic Optimization Using Adaptive Control Vector Parameterization," *Computers & Chemical Engineering*, Vol. 29, No. 8, July 2005, pp. 1731–1751.

[21] de Silva, C., *Vibration and Shock Handbook*, CRC Press, 2005.

[22] Fabien, B. C., "Piecewise Polynomial Control Parameterization in the Direct Solution of Optimal Control Problems," *Journal of Dynamic Systems, Measurement, and Control*, Vol. 135, No. 3, March 2013.

[23] Kraft, D., "A Software Package for Sequential Quadratic Programming," Tech. rep., DLR German Aerospace Center—Institute for Flight Mechanics, Köln, Germany, 1988.

[24] Murua, J., Palacios, R., and Graham, J. M. R., "Applications of the Unsteady Vortex-Lattice Method in Aircraft Aeroelasticity and Flight Dynamics," *Progress in Aerospace Sciences*, Vol. 55, Nov. 2012, pp. 46–72.

[25] Simpson, R. J. S., Palacios, R., and Murua, J., "Induced-Drag Calculations in the Unsteady Vortex Lattice Method," *AIAA Journal*, Vol. 51, No. 7, 2013, pp. 1775–1779.

[26] Gray, J. S., Moore, K. T., Hearn, T. A., and Naylor, B., "Standard Platform for Benchmarking Multidisciplinary Design Analysis and Optimization Architectures," *AIAA Journal*, Vol. 51, No. 10, Oct. 2013, pp. 2380–2394.

6 COPYRIGHT STATEMENT